NATIONAL ADVISORY COMMITTEE FOR AERONAUTICS

TECHNICAL NOTE 3031

PRELIMINARY EXPERIMENTAL INVESTIGATION OF LOW-SPEED TURBULENT BOUNDARY LAYERS IN ADVERSE PRESSURE GRADIENTS

By Virgil A. Sandborn

Lewis Flight Propulsion Laboratory
Cleveland, Ohio

Washington
October 1953

NATIONAL ADVISORY COMMITTEE FOR AERONAUTICS

TECHNICAL NOTE 3031

PRELIMINARY EXPERIMENTAL INVESTIGATION OF LOW-SPEED TURBULENT BOUNDARY LAYERS IN ADVERSE PRESSURE GRADIENTS

By Virgil A. Sandborn

SUMMARY

Measurements of velocity profiles and skin friction in subsonic turbulent boundary layers with adverse pressure gradients are presented. The skin friction was measured by using a local heat-transfer instrument and employing a calibrated relation between heat transfer and skin friction.

The skin friction in an adverse pressure gradient was found to decrease steadily with distance to a value approaching zero for the region of separation. The measured values of skin friction were related to the form factor and momentum thickness of the measured velocity profiles substantially in accordance with the equation of Ludwieg and Tillmann.

Momentum thickness θ and mean velocity-profile-form parameters H computed according to the semiempirical method of Maskell have been compared with the measured quantities. From the agreement it is concluded that the method (which exploits the Ludwieg-Tillmann formula for skin friction) gives results, for the flows investigated, well within a range of engineering accuracy for the predictions of profile parameters, local skin friction, and the point of flow separation; required data for the calculation are the profile parameters at a starting point and the pressure distribution.

INTRODUCTION

Although enough information is available to establish semiempirical equations for predicting the skin friction and mean flow parameters (momentum thickness and displacement thickness) for the case of a zero pressure gradient, no method has as yet been firmly established whereby the skin friction, mean flow parameters, and the flow separation of a turbulent boundary layer can be accurately predicted when the pressure gradient is adverse. The existing data for turbulent boundary layers in adverse pressure distributions have usually been incomplete in that

means for determining the wall shearing stress were not available. Attempts to evaluate the wall shearing stress have proven difficult, with many inconsistencies appearing in the results (refs. 1 and 2).

A theoretical solution of the governing differential equations which will allow the evaluation of the mean quantities is not yet available, since very little is understood of the actual turbulent mechanism. Furthermore, the customary integral approach, which allows the actual detailed mechanism of the flow to be neglected, appears to break down in the adverse pressure flows (ref. 1). It therefore has been necessary to derive semiempirical relations to predict the mean quantities. Several methods have been developed (refs. 3 to 5), but most have serious limitations in the large-pressure-gradient regions. The nonexistence of skin-friction data in adverse pressure gradients has forced most investigators to use the equations developed for flat-plate flow, which must result in serious errors in the region approaching separation.

The most promising semiempirical relations, with respect to simplicity and accuracy, appear to be those derived in reference 6. A review of the existing data for turbulent boundary layers in adverse pressure gradients permitted the introduction of a simple empirical approximation into the momentum equation, which could then be solved directly for the development of the momentum thickness θ in terms of the pressure gradient and some starting value of the momentum thickness (see ref. 6). The specific assumption in the evaluation of momentum thickness was the observation that the momentum equation is insensitive to the variation of the velocity-profile-form factor H so that a simple convenient assumption could be introduced for the variation of H without greatly affecting the calculation of momentum thickness. In order to determine accurately the variation of H in an adverse pressure gradient, an empirical differential equation was constructed which can be solved step-by-step to evaluate H for each point along a flow. The solution for H depends on the value of momentum thickness obtained from the momentum integral and the pressure distribution along the flow.

The calculation of skin friction for adverse pressure gradients has caused the greatest trouble in developing a method for predicting the boundary-layer development. The Ludwieg-Tillmann skin-friction equation (ref. 7), which was developed in recent years, is the only empirical relation determined to fit turbulent skin-friction data for all types of pressure gradient. However, the data obtained in the adverse pressure regions by Ludwieg and Tillmann in order to develop the equation would appear to be the only reliable data in those regions; therefore, no independent check of the equation has as yet been made.

The Ludwieg-Tillmann equation is employed in reference 6 to determine the relations for θ and H and also to predict the skin friction. Although the Ludwieg-Tillmann equation cannot predict the zero value of skin friction expected in a region of separation, it does

decrease to low values of skin friction, which, as suggested in reference 6, may be extrapolated to zero; a point of separation can thus be predicted. This method of predicting separation appears to agree closely with the observed points of separation in the data used in reference 6. The lack of skin-friction measurements in the data precludes independent checks of the predicted wall shearing stress. Unfortunately, the only data available with skin-friction measurements are those of reference 8, which give values much higher than those predicted by the Ludwieg-Tillmann equation. These data must be questionable in that the measured values for the zero-pressure-gradient region of the flow are some 40 percent higher than the established flat-plate values.

Accordingly, independent measurements for the turbulent boundary layer in an adverse pressure gradient (particularly of skin friction) are necessary before a semiempirical calculation method such as that of reference 6 can be established. A preliminary series of measurements in the Lewis 6- by 60-inch subsonic boundary-layer channel is reported herein and compared with the results predicted in reference 6. This investigation was conducted as a part of a general study of the behavior of turbulent boundary layers in adverse pressure gradients. The main purpose of the long-range program is an understanding of turbulent flow separation.

APPARATUS AND PROCEDURE

Description of 6- by 60-Inch Boundary-Layer Channel

The 6- by 60-inch boundary-layer channel was designed for experimental studies of turbulent boundary-layer flows. It is sufficiently versatile to allow a very wide range of flows to be studied - from the fully developed turbulent flow between parallel walls to the development of turbulent-boundary-layer flows in an adverse pressure gradient with resulting separation. A schematic diagram and the two side views of the channel are shown in figure 1.

The tunnel is operated by a 5000-horsepower exhauster approximately 150 feet downstream of the tunnel. The velocity is controlled by a throttling valve near the exhauster inlet, which gives a velocity range up to 120 feet per second at the start of the test section. The channel test wall is a single piece of flat, 1-inch Masonite, 12 feet long. The opposite wall is 12 feet long and constructed of flexible, porous bronze. The walls are set 6 inches apart at the start of the test section and may be expanded to 12 inches at the rear of the channel.

The channel was first designed to take air directly from the atmosphere; however, this was found to yield an unsteady flow because of atmospheric turbulence. In order to steady the flow for measurements, an opening was constructed in the side of the settling chamber (opening indoors), allowing air from the large shop space to act as a surge chamber. By this means, the flow was sufficiently steadied to allow accurate measurements of the velocities to be made.

Ahead of the test section, provisions are made to vary the length of boundary-layer growth by providing five removable, 2-foot-long, 6- by 60-inch channel sections. The inlet section is mounted on wheels to allow for the change in channel length due to the removal of some of the sections. The inlet section has a rapid contraction from 3 feet down to 6 inches in a 2.8-foot run. There are 10 screens (mesh 40) directly upstream of the contraction section.

The pressure gradient on the test wall is adjustable over a large range, primarily by the deflection of the opposite porous wall. Only a small secondary effect on the pressure distribution is provided by suction through the porous wall. The main purpose of the suction is to control the boundary layer on the porous wall, and particularly to prevent flow separation on it. The suction is effected by 16 separate compartments along the length (fig. 1(c)), allowing an arbitrary distribution of suction.

Test conditions. - Since the general program is directed toward an understanding of turbulent flow separation, the flow established in the channel was one in which separation appears to occur on the flat test wall. The tunnel geometry used for the present series of tests is shown in figure 2. With a suction distribution as shown in figure 2 (a constant pressure drop to atmospheric pressure of 25 in. of water was maintained in each suction compartment of the porous wall), and with a free-stream velocity at the start of the test section of approximately 58 feet per second, the flow appeared to separate along the test wall approximately 11 feet from the start of the test wall.

All measurements were taken with a constant Reynolds number per foot of 3.33×10^5 maintained at the entrance of the test section. The free-stream velocity was adjusted for changes in kinematic viscosity from day to day to maintain constant Reynolds number.

Two other flows were also included in the series of measurements to determine the effect of suction through the porous wall. The inlet Reynolds number was kept the same as for the 25-inch-suction case; the suction was then reduced by reducing the pressure drop to 15 inches of water (fig. 2) and finally the suction was eliminated completely.

The two-dimensional character of the flow in the channel was checked by taking velocity surveys from top to bottom of the channel at several positions along the length. The flow was two-dimensional over the lower and center portions of the channel, but a slight thickening of the boundary layer was observed near the top of the channel.

The free-stream turbulent intensity at the start of the test section was approximately 0.4 percent.

Separation indication. - Smoke and china clay were employed in an attempt to indicate the presence of separation. The smoke consisted of fine particles of ammonium chloride generated by bubbling air through ammonium hydroxide and then through hydrochloric acid. The smoke was fed into the boundary layer from a wall probe, which allowed the smoke to stream along very close to the wall.

The china clay method of indicating flow separation (ref. 9) consists in applying a thin coat of white china clay particles to the surface where the flow is to be determined; the actual coating appears as a "white washing" of the surface. A volatile liquid, such as oil of wintergreen, is then sprayed over the coating, which makes the surface appear wet and the clay transparent. The air flow is then established over the surface and allowed to run for some time. If there is flow separation on the surface, a difference in the air-stream evaporation rate should cause the surface to dry more quickly in one region than in another. A line or region of separation will appear as a demarcation between one region in which the volatile liquid has evaporated and another region which is still wet.

Instruments

Pressure measurements. - The mean velocity profiles were measured with a 0.040-inch-diameter total-pressure probe actuated from the top of the channel. The static pressure was obtained from wall static orifices (0.025-in. diam.) along the test wall. A static-pressure probe consisting of a 0.020-inch-diameter tube with two 0.010-inch-diameter static holes was also employed to measure the change in static pressure through the boundary layer. No corrections were made for effects of the turbulence on the pressure readings or for variation of static pressure through the boundary layer. All pressure readings were recorded with a water micromanometer with a least count of 0.001 inch of water.

Heat transfer - skin friction instrument. - A technique for measuring local skin friction by means of a calibrated relation between the shearing stress and heat transfer has been developed (ref. 10). This instrument measures the amount of heat a given shear flow will transfer away from a small heated segment of wall. A modified version of this instrument was employed in the present investigation (fig. 3(a)).

The instrument developed in reference 10 consisted of a copper block with a small electric heater. The block was cemented to a very thin celluloid diaphragm, through which the heat was transferred. The block was set in a dead-air region which formed the heat insulation for the instrument. The thin celluloid diaphragm transferred very little heat to the casing and, because of its thin dimension, had little effect on the heat transfer to the air. A thermocouple was set near the heat-transfer surface to measure the temperature of the block.

The instrument used in the present investigation consists of two pads, A and B (fig. 3(a)); pad A is a reference element that is considered to assume the temperature of the unheated wall, and pad B is the heating element. The pads are made of a low-melting-point alloy, so that they may be cast directly into the Lucite case. A Nichrome wire heating element is set in pad B. Imbedded in the surfaces of the pads is an iron-constantan thermopile consisting of six thermocouples connected in series. The cold junctions of the thermocouples are in the surface of pad A and the hot junctions in pad B. With the thermopile it is possible to measure small temperature differences, resulting in accuracies of approximately 1 percent in the temperature difference between pads A and B.

In the operation of the instrument, the temperature difference between the heated pad and, in effect, the wall was obtained directly from the measure of the electromotive force generated by the thermopile. All the power input to the heating element was considered to be transferred to the air stream; the power input was determined by voltage and current measurements. Figure 3(b) shows the circuit used to supply the heating element and the two readings used to determine the power input.

Calibration. - In reference 10 a theoretical relation for the rate of heat transfer for the instrument was obtained in terms of the local wall shearing stress. The specific relation obtained was

$$Nu = 0.807\,\bar{L}^{2/3} \tag{1}$$

where Nu = Nusselt number $= \frac{Q}{A\Delta T}\frac{L}{k}$ and $\bar{L} = \left(\frac{\tau_0}{\rho}\right)^{1/2}\left(\frac{C_p \rho L^2}{\nu k}\right)^{1/2}$. (A list of symbols is given in appendix A.) This relation was obtained under the assumptions that the small perturbation in temperature due to the instrument constituted a small thermal boundary layer within the main boundary layer and was limited (except far downstream) to a region very near the wall. Thus the velocity profile in the affected region was replaced by its tangent at the wall, and turbulent heat transfer and momentum transfer were neglected.

The actual heat transfer measured by the instruments consists, however, of two parts; the major part is that transferred to the air stream by forced convection as assumed by Ludwieg, and, secondly, a leakage flow is transferred internally to the walls of the case, since the Lucite is an imperfect insulator. Because of the presence of this internal heat leakage and perhaps other imperfections in the instruments, the theoretical relation predicted between the heat transfer and the skin friction cannot be expected to apply directly to a particular instrument. The instrument relation depends instead upon a direct calibration between the measured rate of heat transfer and the wall shearing stress.

The heat-transfer instruments were calibrated in a fully developed turbulent channel flow in order to facilitate the measurement of the wall shearing stress. The calibration flow was obtained by placing the 6- by 60-inch boundary-layer channel walls parallel and adding all available channel sections to give a channel 22 feet in length.

In order to indicate the existence of fully developed turbulent channel flow at the rear of the channel, a heat-transfer instrument was placed at several stations along the last 4 feet. The existence of constant shear stress, a characteristic of such a flow, was verified by noting that the rate of heat transfer was the same at all stations along the last 4 feet. The wall shearing stress was then determined directly from a measure of the static-pressure gradient in the direction of the mean flow (x-direction), since the equilibrium of forces in the x-direction gives

$$\tau_0 = h \frac{dp}{dx} \tag{2}$$

where h is the channel half width.

Twelve heat transfer - skin friction instruments were mounted in special lapped brass fittings along the center portion of the channel test wall. The instruments were operated at constant heat-input settings to minimize the effect of internal heat leakage of the instrument; also, the air temperature for all measurements was approximately the same as the calibration flow temperature, thus minimizing any effect due to change in environment. The instruments were operated one at a time and were always operated from the back to the front of the channel.

Figure 4 shows a typical calibration relation obtained for the heat transfer - skin friction instruments. The calibration shows a linear relation between the experimental parameters, but not that predicted in reference 10; however, as pointed out previously, the exact theoretical relation could not be expected to apply directly because of such errors as internal heat leakage or free-convection effects, or both; the principal effect is the substantial zero shift.

The first attempt to calibrate the heat transfer - skin friction instrument was to set the wall of the 6- by 60-inch channel so that the first two stations along the test wall would be in a zero-pressure-gradient boundary-layer region. The wall shearing stress for calibration was obtained by evaluating the momentum thickness from measured velocity profiles and then applying Falkner's equation (ref. 11)

$$c_f = \frac{0.01306}{(R_\theta)^{1/6}} \tag{3}$$

where

$$c_f = \frac{\tau_0}{\frac{1}{2}\rho U_1^2}$$

The measured points are shown in figure 4.

The reason for disagreement between the two types of calibration (fully developed turbulent flow and flat-plate boundary-layer flow) is not known. Use of the Ludwieg-Tillmann equation gives skin-friction values very close to those of Falkner's equation, and the velocity profiles agree very closely with those observed by other experimenters for flat-plate flow. This discrepancy between calibrations points up the main difficulty in the use of this type of instrument, which is the establishment of a known shear stress to use for calibration.

For the flows investigated herein the calibration for fully developed flow was used, since it is obtained directly from measurements and a relation between pressure and skin friction that comes directly from the equations of motion; thus, no empirical results are needed in the skin-friction evaluation. Also, the final resulting skin-friction measurements come closer to the values predicted by the Ludwieg-Tillmann equation and would appear to indicate more closely the region of observed separation. Because of the question of calibration, the measurements of skin friction must be considered as trends and qualitative results rather than as absolute magnitudes.

DISCUSSION OF RESULTS

Mean Velocity Distribution and Separation

The pressure distributions for the three flows investigated are shown in figure 5, where the free-stream dynamic pressures divided by the free-stream dynamic pressure at the start of the test section are plotted against distance. Also included in figure 5 is the pressure distribution studied in reference 8 for a similar flow.

The mean velocity variations through the boundary layer at different distances for the three flows are shown in figure 6. Figure 7 shows the velocity profile obtained at the last station (x = 10.67 ft) for the highest-suction case compared with the profile obtained in reference 8 at the observed separation point. Because of the fluctuations in total pressure in the region near separation, considerable scatter was observed in the velocity measurements near the wall.

The mean static-pressure variation through the boundary layer was found to be less than 1 percent in the region approaching separation, with only a slightly larger variation being observed near separation.

The computed boundary-layer parameters, namely, displacement thickness δ^*, momentum thickness θ, and form factor H, are shown in figure 8. The form factor H has been suggested as an indicator of separation; a literature search (ref. 12) indicated that separation would occur for a value of H in the range between 1.8 and 2.6. It was pointed out in reference 3 that the rate of change of H in the flow direction, dH/dx, may be the determining factor; however, reference 3 indicated that separation should occur for a value of H greater than 2.6. Figure 8(c) shows H to have reached approximately 2.8 for the highest-suction case where the flow is believed to be separating (see following section); this has been compared (fig. 7) with the value 2.8 observed in reference 8 at the separation point.

The discrepancy in the use of H as an empirical guide for predicting separation appears systematic. The value H = 2.6 was obtained from observations of separation on airfoils having short length of boundary-layer growth and large pressure gradients, while separation occurred herein and in reference 8 after a great length of boundary-layer growth and small pressure gradients. These results indicate that the value of H at separation is a function of boundary-layer growth or the pressure gradient, or both; thus H cannot be used by itself as a precise indicator of separation.

The determination of a line of separation was found to be impossible, as the flow indicators fail to yield definite results. Instead of indicating an abrupt flow deflection outward from the wall, the only effect of the smoke was an increase in the diffusion rate in a 6-inch-wide region some 11 feet from the start of the test wall. The high rate at which the smoke streams diffused in the region approaching separation made it difficult to observe once separation was reached. The use of china clay also indicated a slight decrease in the evaporation rate behind the same region indicated by the smoke. However, the clay did not give a precise indication of separation, as the variation of evaporation rates was so small that it was necessary to apply the volatile liquid uniformly to the surface, which proved difficult because of the narrow confines of the channel walls.

Although more evidence is necessary before definite facts can be established regarding the separation region, a few trends may be inferred from the observations. The flow indicators seem to indicate that the position of separation was a time-dependent phenomenon; thus, on a time average, no sharp line between separated and unseparated flow exists. The increase in diffusion rate and the large scatter observed in total-pressure measurements indicate that the turbulent intensities are very large in the region of separation. The use of total-pressure probes makes the recording of reverse velocities impossible, and the high-intensity turbulence near the wall in the separation region makes the velocity readings observed questionable; however, no indication of reverse flow was observed by releasing smoke from the wall probe downstream of the separation region.

Comparison of Experimental Values with Semiempirical Relations

The values predicted by the method constructed in reference 6 (see appendix B) for the pressure gradients investigated herein are compared in figures 9 and 10 with the values obtained from experimental measurements. The two flows in which suction was employed through the porous wall are seen to agree very well in the values of θ and H with those predicted in reference 6. The disagreement for the no-suction case is possibly due to a nonuniform development of the porous-wall boundary layer - which in this case is very thick - disturbing the two-dimensionality of the flow.

The comparison of the predictions of reference 6 with those of the method presented in reference 3 was performed in reference 6; the two methods showed good agreement. The method of reference 6, however, is simpler to apply, because it does not require numerical solutions of pairs of simultaneous differential equations.

Wall Shearing Stress

The heat transfer - skin friction instruments were used to measure the local shearing stress along the test wall for the three flows investigated. Figure 12 shows the results obtained when the x-distance is measured from the start of the test section. The results (figs. 12(a) and 12(b)) show the wall shearing stress tending toward zero in the adverse pressure gradients. The trend agrees with the hot-wire measurements of reference 8 and also that of the Ludwieg-Tillmann equation

$$c_f = 0.246 \times 10^{-0.678H} R_\theta^{-0.268} \tag{4}$$

This result, in addition, supports conclusions reached in references 1, 13, and 14 that, unless extended to include turbulent perturbation terms, the momentum method is of questionable value in the regions of adverse gradient (fig. 12(a)), where it indicates a trend opposite to that observed by the hot-wire or heat-transfer method. While the method of evaluating the skin friction in the present report did not give quantitative results (there may be a small systematic error due to some inconsistency encountered in the instrument calibration), it does give added strength to the discarding of results obtained from the conventional momentum integral approach for large adverse pressure gradients.

The reason for the failure of the momentum integral method is not yet completely established. Recent investigations (refs. 1, 12, and 13) have attempted to treat more general integral relations taking into account the turbulent fluctuation terms. The analysis of reference 1 indicated that the mean flow and the anisotropic low-frequency turbulence terms neglected in the Prandtl boundary-layer assumptions had little or no effect on the evaluation of skin friction, while the terms that appear to be important are the turbulent contributions to the momentum deficiency thickness. The effect of the normal turbulent stress component $\rho\overline{u^2}$, which appears in the turbulent expression for θ, was investigated in reference 13. The results of this investigation indicated that the gradient of this term will be large in the region near separation and should not be neglected. Reference 14 indicates the same results.

The heat-transfer instruments appear to have reached a certain limiting minimum reading in the region near separation (fig. 12(a)). This limiting value of heat transfer is greater than the value observed for the no-flow condition (zero wall shearing stress), which would suggest that the mean wall friction has not fallen to zero. Actually, the instrument may be expected to deviate from the theory at very low flow rates, because of additional heat transfer by means of a superimposed free convection. The mean wall friction may well be zero in this region, while the highly turbulent flow around the separation increases the free-convection heat loss.

Included in figure 12 are the values of local skin friction evaluated from the velocity profiles by the semiempirical Ludwieg-Tillmann equation (4). The measured skin-friction values and those calculated by the Ludwieg-Tillmann equation fail to show qualitative agreement only in the case of flow without suction. As noted before, this discrepancy is probably to be attributed to the boundary layer on the porous wall influencing the two-dimensionality of the flow. The two flows in which there was suction along the porous wall, where no interference between the boundary layers occurred, agree with the Ludwieg-Tillmann predictions within approximately 20 percent over the regions investigated, excluding separation. As noted in the INTRODUCTION, the wall shearing stress measured in reference 8 with the hot wire failed to check the Ludwieg-Tillmann equation; however, the difference between the two results was approximately a constant multiplicative factor (ref. 1). Reference 8 offers the only available measurements of skin friction for a turbulent boundary layer in an adverse pressure gradient that are not based on the discredited form of momentum balance, except those used by Ludwieg and Tillmann to evaluate their equation; however, the disagreement of the measurements of reference 8 with established flat-plate values of skin friction in the region of zero pressure gradient would appear to indicate a systematic error in these data.

Values of skin friction calculated from the semiempirical predictions of H and R_θ in reference 6 are also included in figure 12. In the two cases where suction was used, the results give good qualitative agreement with the measured values. As noted before, the Ludwieg-Tillmann skin-friction equation, which is utilized in the method of reference 6, cannot predict a zero skin-friction coefficient. It is therefore necessary to extrapolate the curve to the point of zero c_f in order to determine the separation point. In figure 12(a) the results of the extrapolation of the predictions of reference 6 appear to be in agreement with the observed region of flow separation.

CONCLUDING REMARKS

The skin friction in an adverse pressure gradient is found to decrease steadily with distance to a value approaching zero for the region of separation. This trend agrees with that of the hot-wire measurements of Schubauer and Klebanoff. In addition, the results support the contention of Goldschmied and others that the reverse trend apparently indicated by the momentum method is spurious.

The measured skin friction agrees fairly well with that predicted by the semiempirical Ludwieg-Tillmann formula when measured values of H and R_θ are used:

$$c_f = 0.246 \times 10^{-0.678H} R_\theta^{-0.268}$$

(where c_f is local skin-friction coefficient, H is mean velocity-profile-form parameter, and R_θ is Reynolds number based on momentum thickness). The precision of the measurements is insufficient, however, to do more than confirm the qualitative correctness of the formula.

Maskell's semiempirical method agrees very well with the values of θ, and well with the values of H measured, when known values of θ and H at some initial station are employed. In the prediction of values of local skin friction by use of the Ludwieg-Tillmann equation and the point of flow separation, the method appears to be within the range of engineering accuracy for the values of Reynolds number and pressure gradient investigated.

Lewis Flight Propulsion Laboratory
National Advisory Committee for Aeronautics
Cleveland, Ohio, July 30, 1953

APPENDIX A

SYMBOLS

A	area of heat-transfer surface
c_f	local skin-friction coefficient, $\tau_0 \Big/ \frac{1}{2} \rho U^2$
c_p	specific heat of air at constant pressure
H	mean velocity-profile-form parameter, δ^*/θ
h	channel half width, 3 in.
k	thermal conductivity of air
L	length of heat-transfer surface in the mean flow direction
$\bar{L}$	dimensionless shear stress function, $\left(\frac{\tau_0}{\rho}\right)^{1/2}\left(\frac{c_p \rho L^2}{\nu k}\right)^{1/2}$
Nu	Nusselt number, $\frac{Q}{A}\frac{L}{\Delta T\, k}$
p	static pressure
Q	rate of heat transfer
q	dynamic pressure, $\frac{1}{2} \rho U^2$
R_θ	Reynolds number, based on momentum thickness, $\frac{\rho U_1 \theta}{\mu}$
$r(H)$	function of velocity-profile-form parameter, $-0.30H + 0.32$
$s(H)$	function of velocity-profile-form parameter, $-0.15(H-1.2)$
ΔT	temperature rise of heat-transfer surface
$t(H)$	function of velocity-profile-form parameter, $-0.15(2H-1)$
U	local mean velocity
$\overline{u^2}$	mean square of turbulent velocity fluctuation in direction of local mean velocity

x direction of mean flow (usually measured in feet from start of test wall)

y direction perpendicular to boundary and mean flow

α constant, 0.01173

β constant, 4.200

Γ pressure gradient parameter, $\frac{0.246}{c_f}\frac{\theta}{U_1}\frac{dU_1}{dx}$

δ^* displacement thickness, representation of the mass-flow deficiency, $\int_0^\infty \left(1 - \frac{U}{U_1}\right) dy$

Θ_1 function of momentum thickness, $\theta\, R_\theta^{0.2155}$

θ momentum thickness, representative of the mean-flow momentum deficiency, $\int_0^\infty \frac{U}{U_1}\left(1 - \frac{U}{U_1}\right) dy$

μ viscosity of air

ν kinematic viscosity of air, μ/ρ

ρ density of air

τ_0 local wall shearing stress

$\Phi(0,H)$ function of the velocity-profile-form parameter (plotted in fig. 10)

Subscripts:

0 value taken at first station near start of test wall

1 free-stream condition (beyond the edge of the boundary where viscous effects are neglected)

APPENDIX B

SEMIEMPIRICAL RELATION FOR TURBULENT-BOUNDARY-LAYER DEVELOPMENT

Calculation of Momentum Thickness

Starting with the boundary-layer momentum equation, it was noted in reference 6 that the solution did not depend on an accurate knowledge of the variation of H. If a simple approximation for H is introduced, the momentum equation may be solved to determine θ directly. The relation obtained is

$$(\Theta_1 U_1^{\beta})_x - (\Theta_1 U_1^{\beta})_{x_0} = \alpha \int_{x_0}^{x} U_1^{\beta} \, dx \qquad \text{(B1)}$$

where

$$\Theta_1 = \theta R_\theta^{0.2155}$$

$$\alpha = 0.01173$$

$$\beta = 4.200$$

and x_0 is taken as the starting point where θ_{x_0} can be determined either from a direct measurement of the velocity profile or from laminar-boundary-layer calculations up to the point of flow transition, since θ is a continuous function through transition.

The solution of equation (B1) requires only the knowledge of the free-stream velocity distribution and some means of determining a starting value of θ.

Profile Parameter

The development of the profile parameter H in adverse pressure gradients is defined by an empirical differential equation:

$$\theta \, R_\theta^{0.268} \frac{dH}{dx} = \Phi(0,H) + r(H)\Gamma \qquad (0 > \Gamma > \Gamma_i) \qquad \text{(B2a)}$$

$$= s(H) + t(H)\Gamma \qquad (\Gamma < \Gamma_i) \qquad \text{(B2b)}$$

where

$$\Gamma = \frac{0.246}{c_f} \frac{\theta}{U_1} \frac{dU_1}{dx}$$

$$\Gamma_i = \frac{s(H) - \Phi(0,H)}{0.17}$$

$$-r(H) = 0.30H - 0.32$$

$$-s(H) = 0.15(H - 1.2)$$

$$-t(H) = 0.15(2H - 1)$$

and $\Phi(0,H)$ is given as a plot against H in reference 6 and is reproduced in figure 11.

The solution of equation (B2) requires the knowledge of θ obtained from equation (B1) and a starting value of H. The value of c_f is determined from the Ludwieg-Tillmann equation:

$$c_f = 0.246 \times 10^{-0.678H} \times R_\theta^{-0.268} \qquad \text{(B3)}$$

The pressure distribution must also be known. Solving equation (B2) yields a value of dH/dx which can then be extrapolated to a new point a small distance Δx downstream. The process is repeated for each successive Δx until the complete distribution of H is obtained.

For favorable or zero pressure gradients ($\Gamma \geq 0$), the empirical relation

$$H = 1.754 - 0.149 \log_{10} R_\theta + 0.01015 (\log_{10} R_\theta)^2 \qquad \text{(B4)}$$

is used to determine H directly.

In a step-by-step calculation such as equation (B2), the accuracy is improved by going to smaller and smaller steps, but at the expense of increased labor. In the present calculation, steps of approximately 0.75 foot were finally adopted; it was found that the values of H calculated with steps twice this size differed appreciably near separation.

REFERENCES

1. Goldschmied, Fabio R.: Skin Friction of Incompressible Turbulent Boundary Layers under Adverse Pressure Gradients. NACA TN 2431, 1951.

2. Wieghardt, K., and Tillmann, W.: On the Turbulent Friction Layer for Rising Pressure. NACA TM 1314, 1951.

3. von Doenhoff, Albert E., and Tetervin, Neal: Determination of General Relations for the Behavior of Turbulent Boundary Layers. NACA Rep. 772, 1943. (Supersedes NACA WR L-382.)

4. Buri, A. (M. Flint, trans.): A Method of Calculation for the Turbulent Boundary Layer with Accelerated and Retarded Basic Flow. R.T.P. Trans. No. 2073, Ministry Aircraft Prod. (British).

5. Tetervin, Neal, and Lin, Chia Chiao: A General Integral Form of the Boundary-Layer Equation for Incompressible Flow with an Application to the Calculation of the Separation Point of Turbulent Boundary Layers. NACA Rep. 1046, 1951. (Supersedes NACA TN 2158.)

6. Maskell, E. C.: Approximate Calculation of the Turbulent Boundary Layer in Two-Dimensional Incompressible Flow. Rep. No. Aero. 2443, British R.A.E., Nov. 1951.

7. Ludwieg, H., and Tillmann, W.: Investigation of the Wall-Shearing Stress in Turbulent Boundary Layers. NACA TM 1285, 1950.

8. Schubauer, G. B., and Klebanoff, P. S.: Investigation of Separation of the Turbulent Boundary Layer. NACA Rep. 1030, 1951. (Supersedes NACA TN 2133.)

9. Richards, E. J., and Burstall, F. H.: The "China Clay" Method of Indicating Transition. R. & M. No. 2126, British A.R.C., Aug. 1946.

10. Ludwieg, H.: Instrument for Measuring the Wall Shearing Stress of Turbulent Boundary Layers. NACA TM 1284, 1950.

11. Falkner, V. M.: A New Law for Calculating Drag. Aircraft Eng., vol. XV, no. 169, Mar. 1943, pp. 65-69.

12. Granville, Paul S.: A Method for the Calculation of the Turbulent Boundary Layer in a Pressure Gradient. Rep. 752, Navy Dept., The David W. Taylor Model Basin, Wash. (D.C.), May 1951.

13. Bidwell, Jerold M.: Application of the von Kármán Momentum Theorem to Turbulent Boundary Layers. NACA TN 2571, 1951.

14. Newman, B. G.: Skin Friction in a Retarded Turbulent Boundary Layer Near Separation. Rep. A.73, Dept. of Supply, Aero. Res. Lab., Commonwealth of Australia, Nov. 1950.

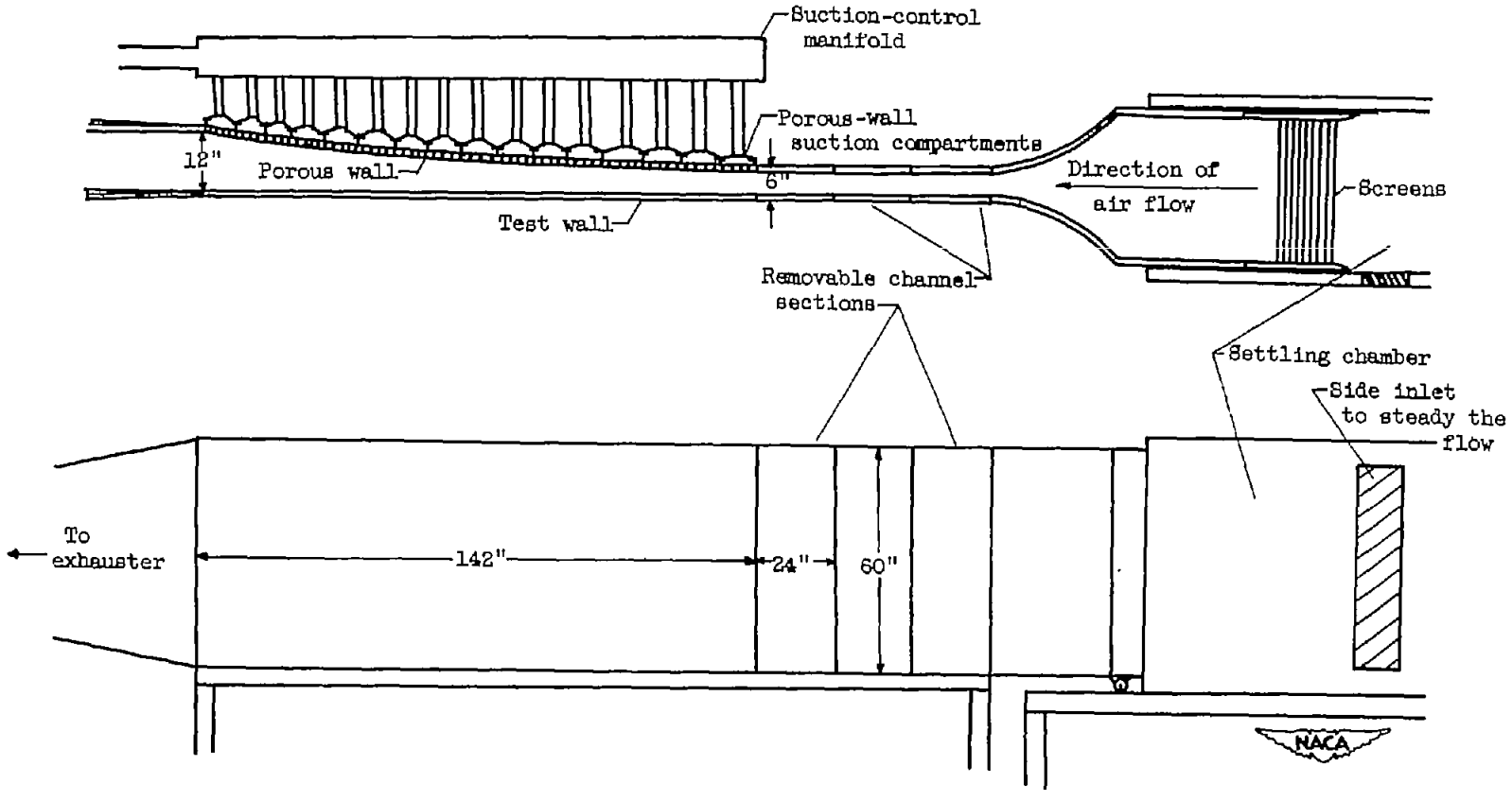

(a) Schematic diagram.

Figure 1. - Views of 6- by 60-inch subsonic boundary-layer channel.

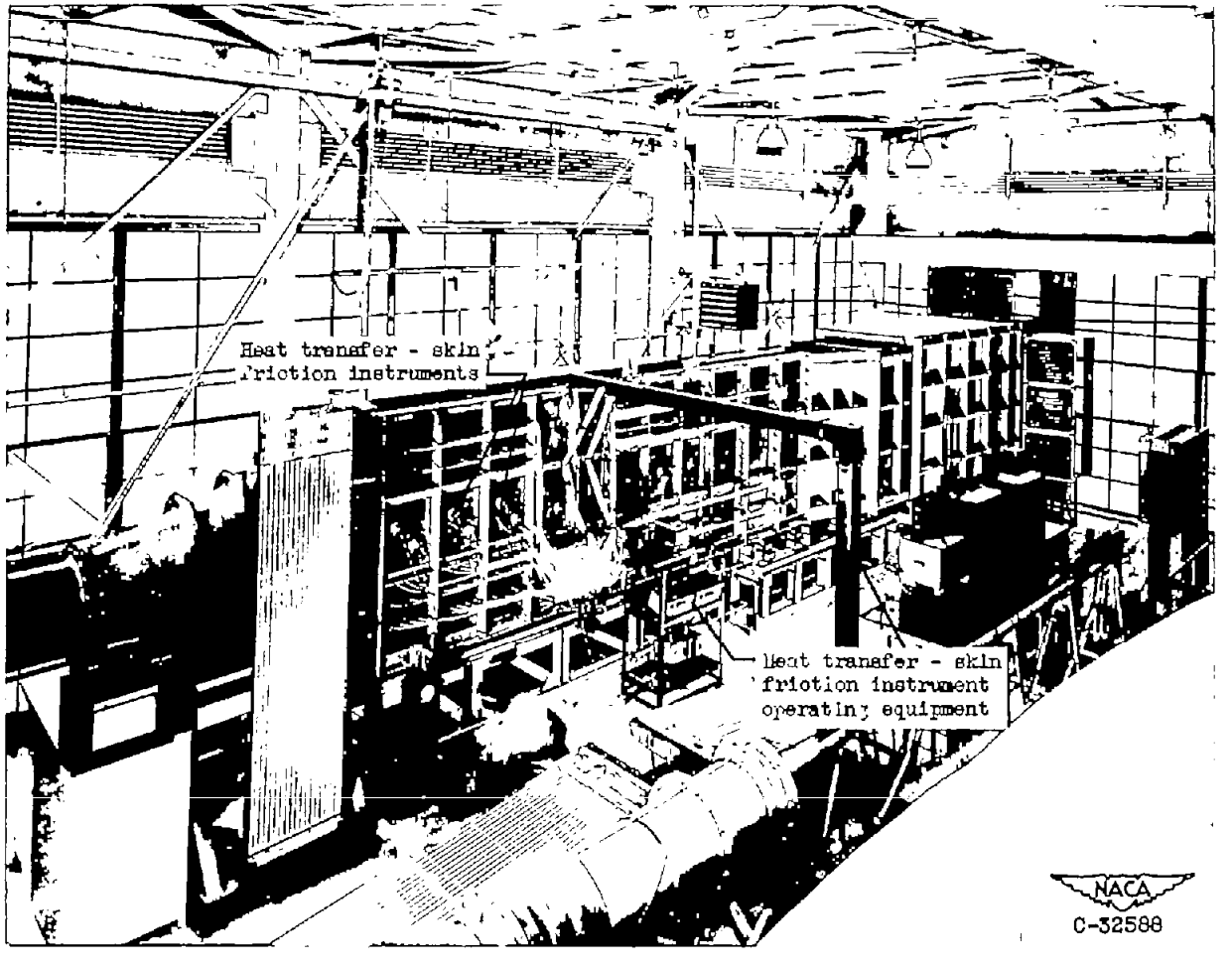

(b) Along test wall side.

Figure 1. - Views of 6- by 60-inch subsonic boundary-layer channel.

(c) Suction compartments along porous wall.

Figure 1. - Concluded. Views of 6- by 60-inch subsonic boundary-layer channel.

x, ft	y, in.	x,ft	y, in.
0.75	6.025	6.75	8.500
1.50	6.075	7.50	9.000
2.25	6.200	8.25	9.500
3.00	6.425	9.00	10.000
3.75	6.750	9.75	10.500
4.50	7.100	10.50	11.000
5.25	7.525	11.25	11.500
6.00	8.000	12.00	12.00

Channel-wall coordinates

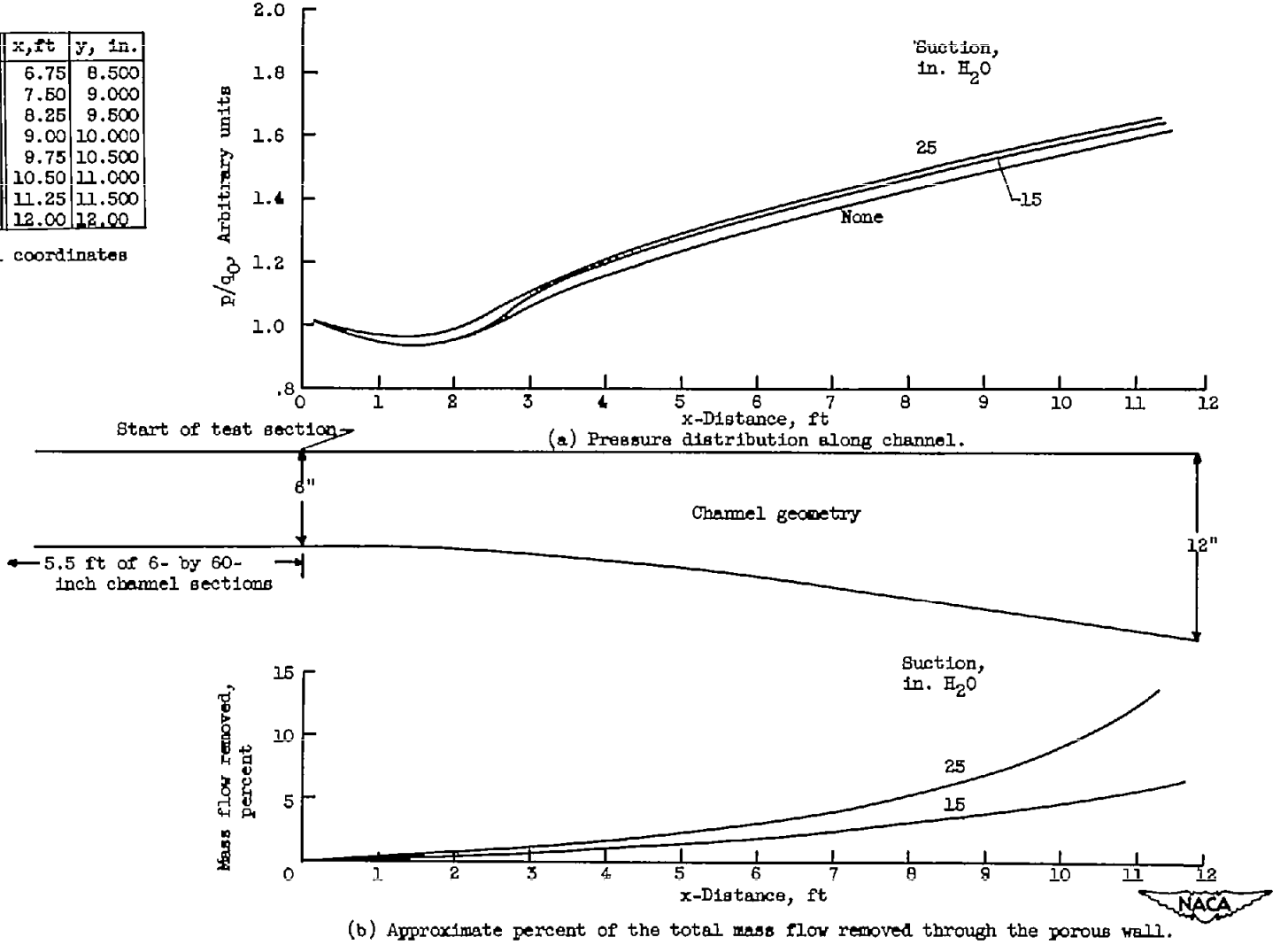

(b) Approximate percent of the total mass flow removed through the porous wall.

Figure 2. - Tunnel geometry and flow conditions.

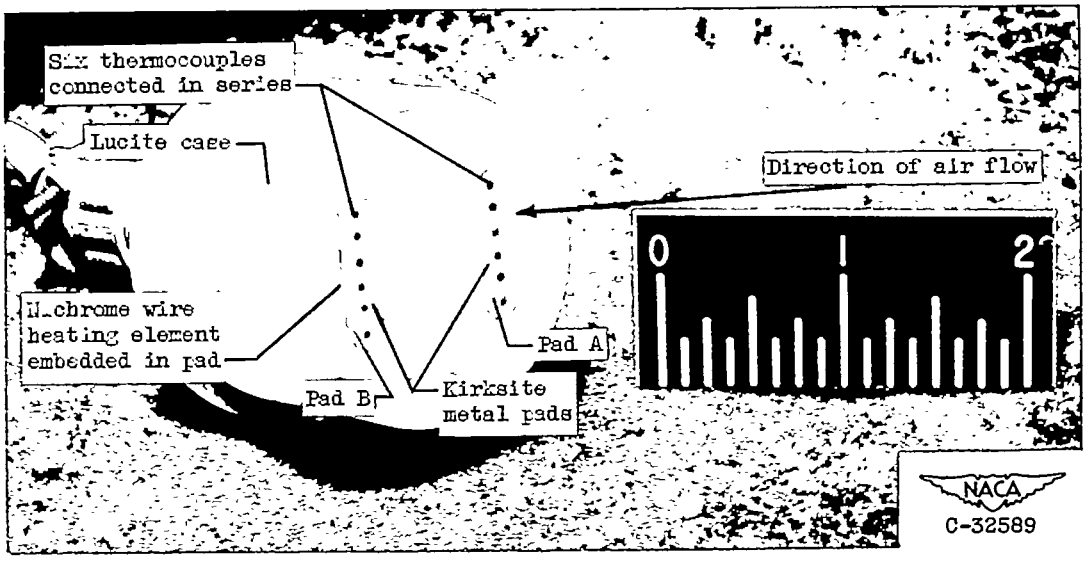

(a) Photograph.

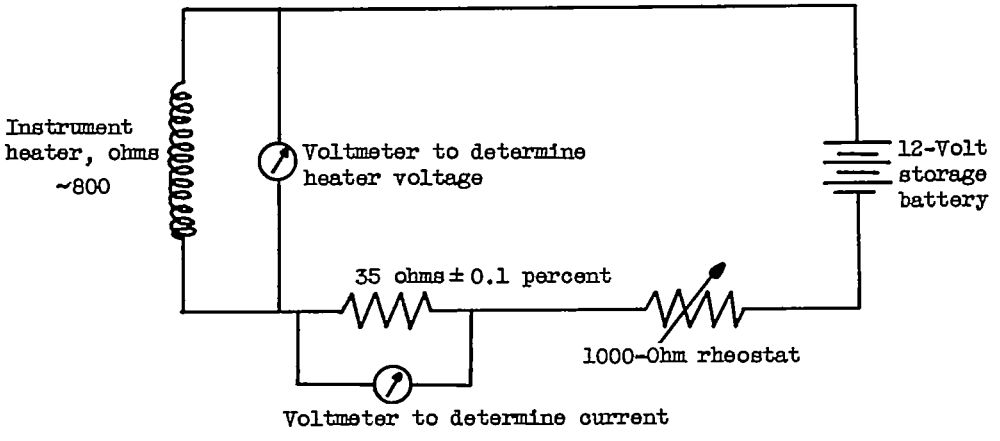

(b) Diagram of heating circuit.

Figure 3. - Heat transfer - skin friction instrument.

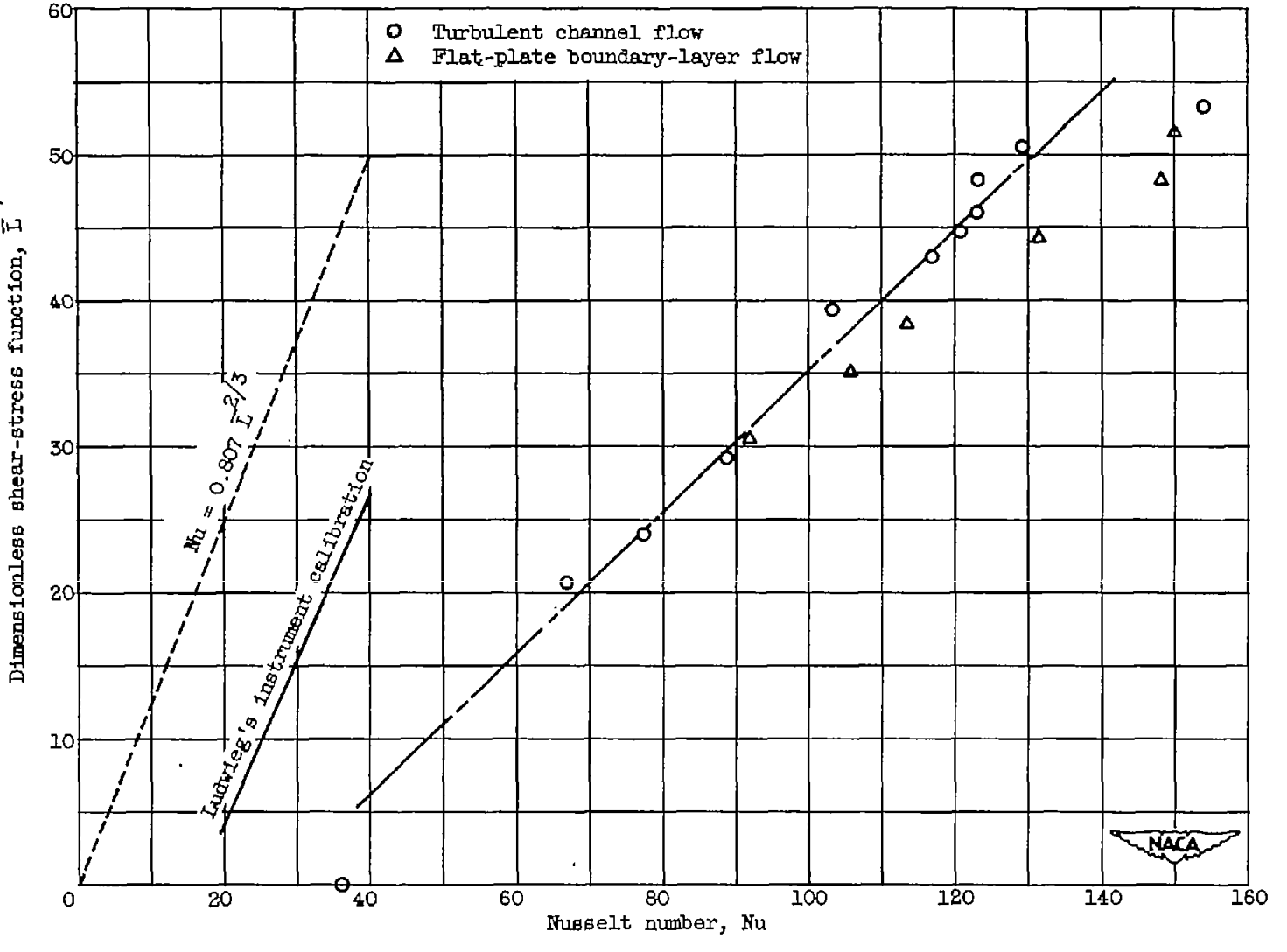

Figure 4. - Calibration of heat transfer - skin friction instrument.

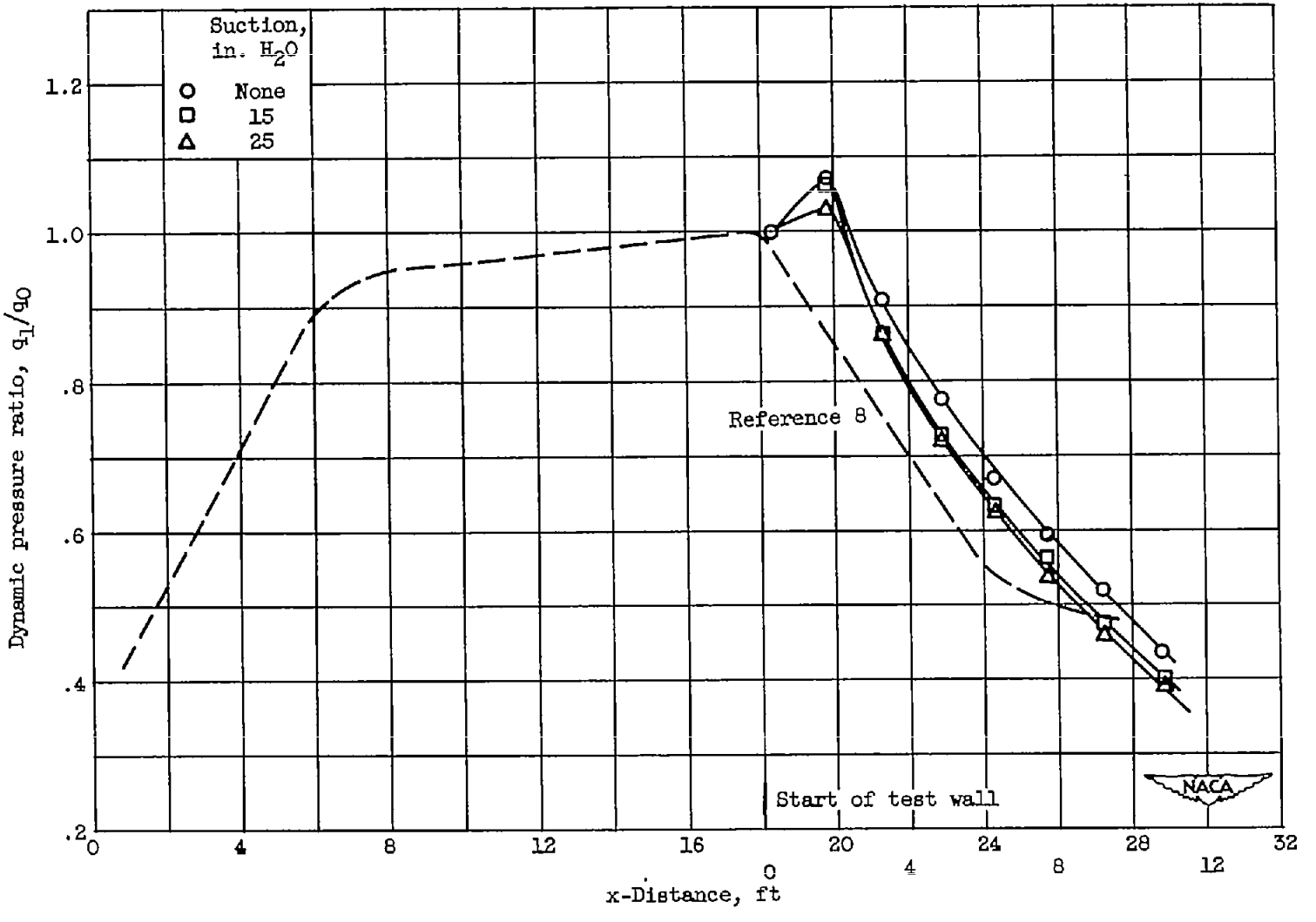

Figure 5. - Comparison of pressure distributions with that of reference 8. Dynamic pressure, 3.74 pounds per square foot; approximate temperature range, 82° to 95° F.

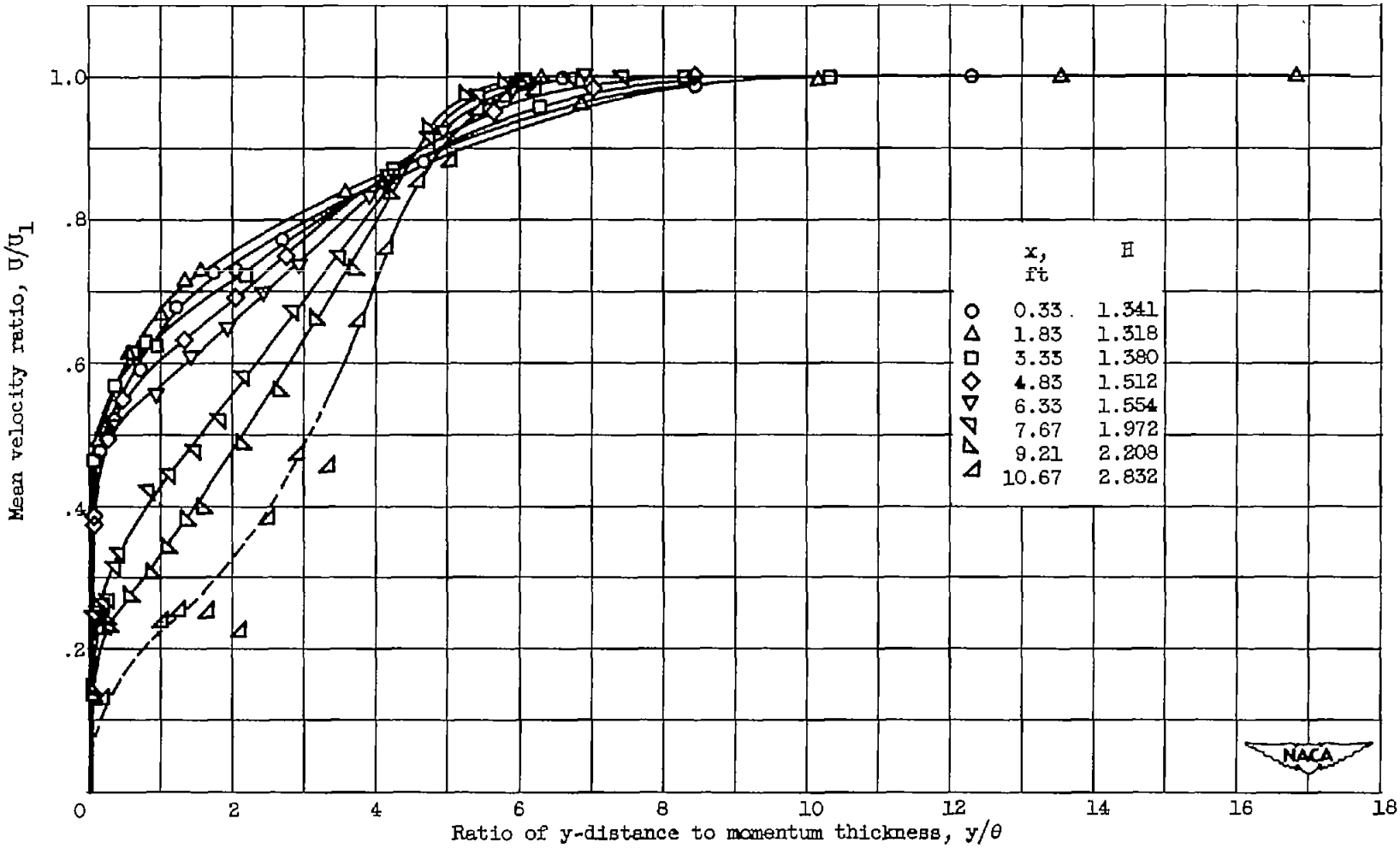

(a) Suction, 25 inches of water.

Figure 6. - Velocity profiles along the test wall.

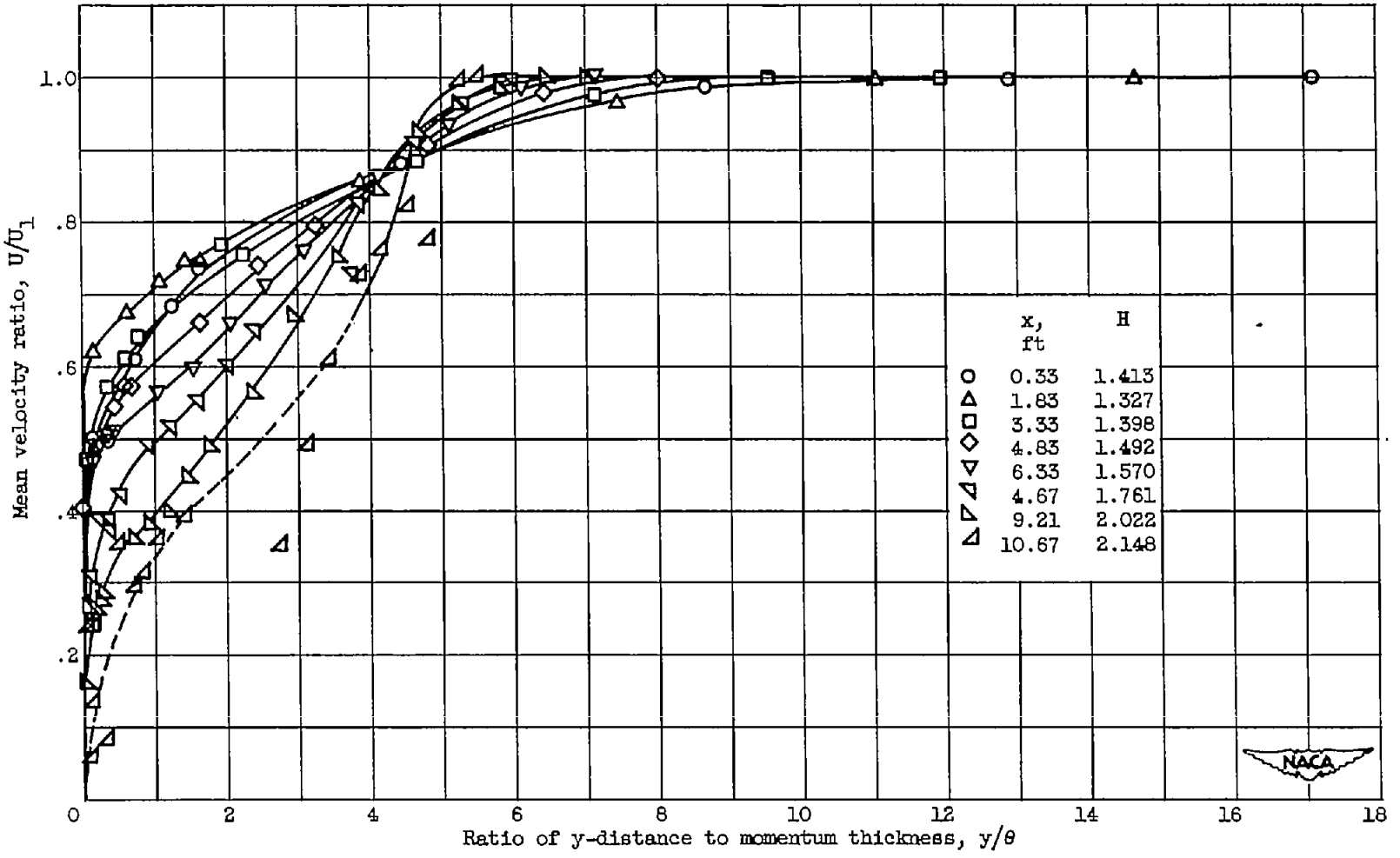

(b) Suction, 15 inches of water.

Figure 6. - Continued. Velocity profiles along the test wall.

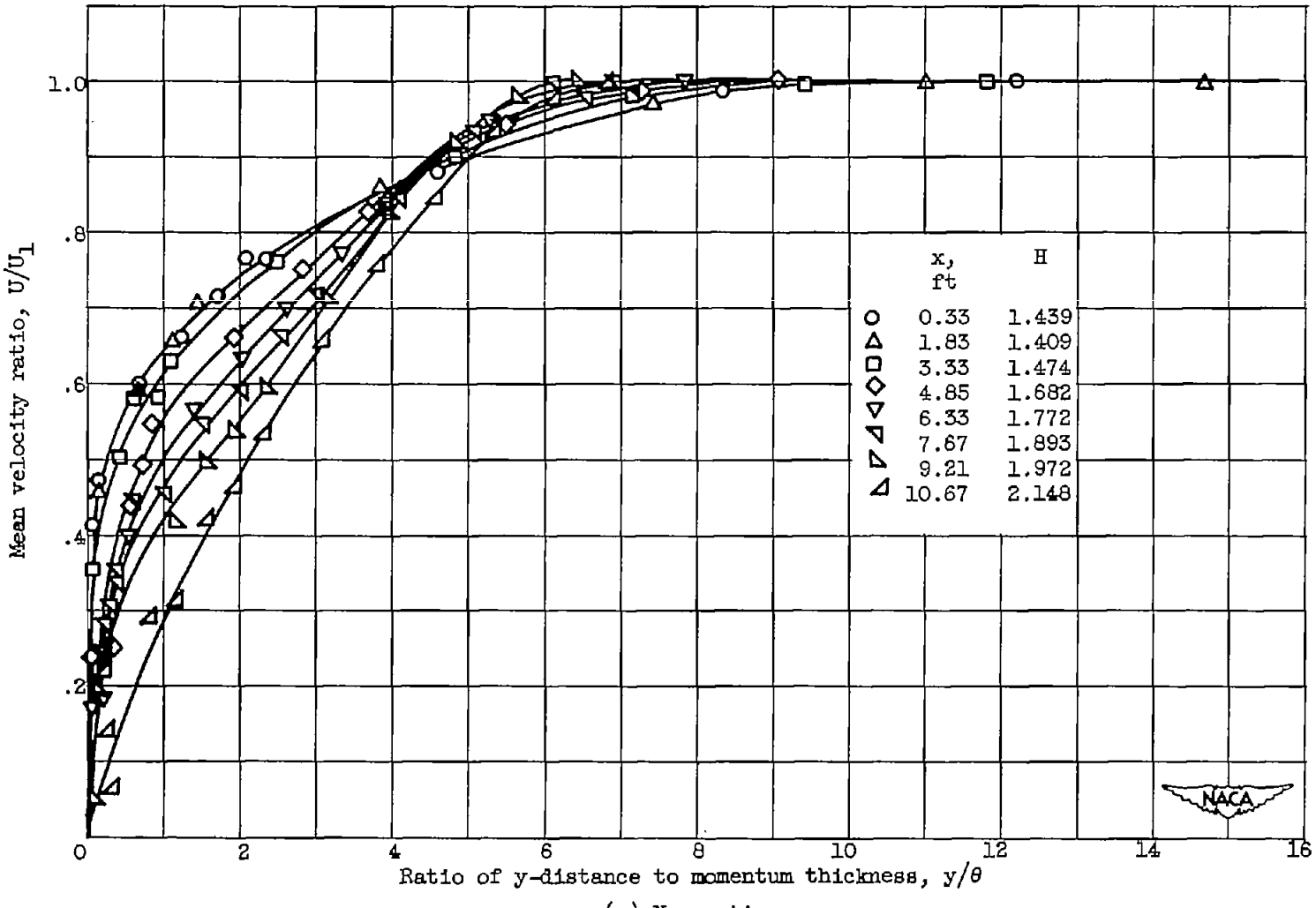

(c) No suction.

Figure 6. - Concluded. Velocity profiles along the test wall.

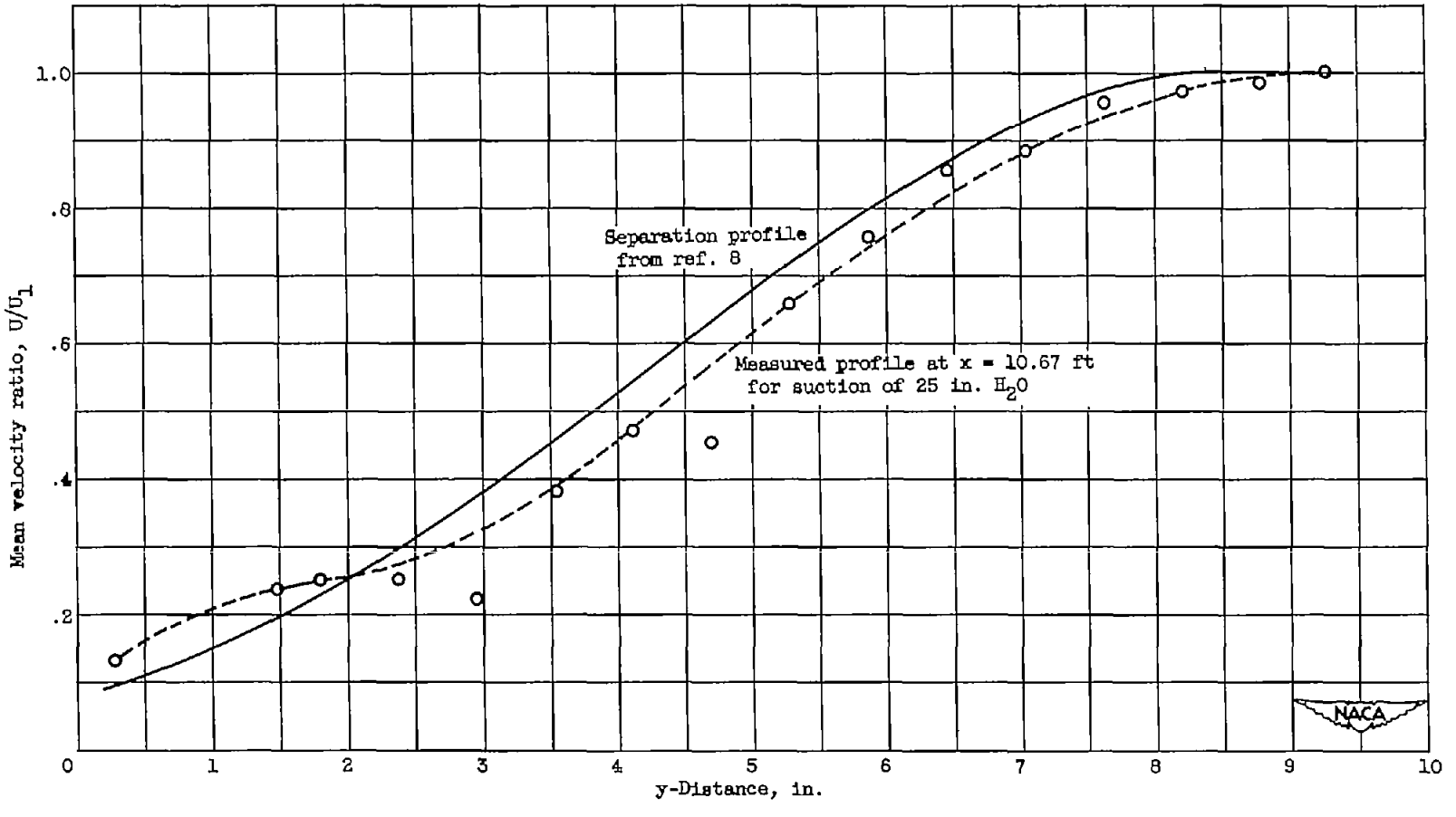

Figure 7. - Comparison of velocity profile in the region of separation with that of reference 8. Mean velocity-profile-form factor, H, 2.8.

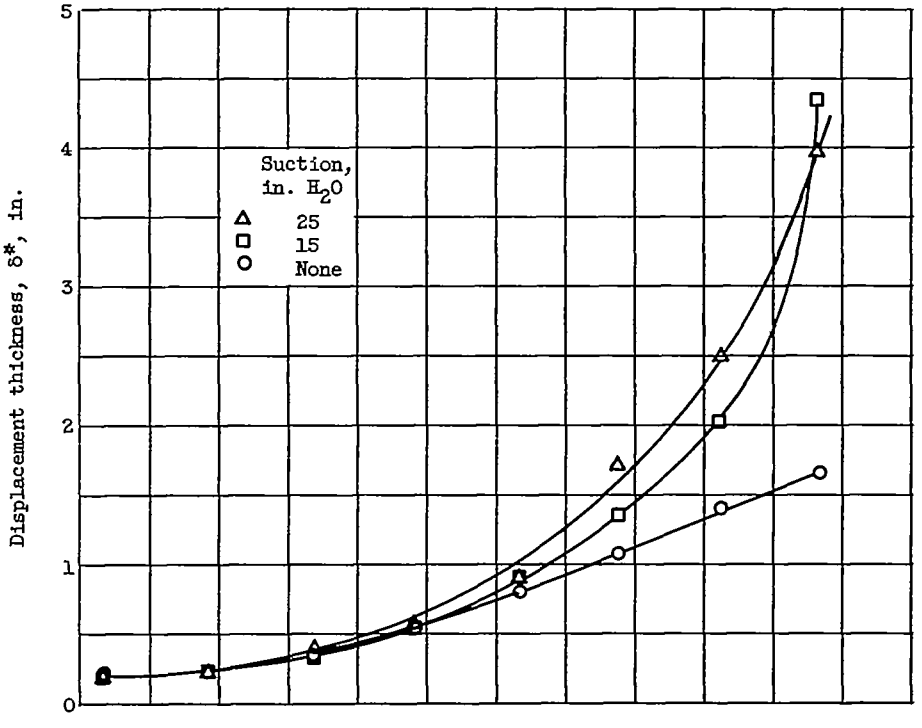

(a) Displacement thickness growth.

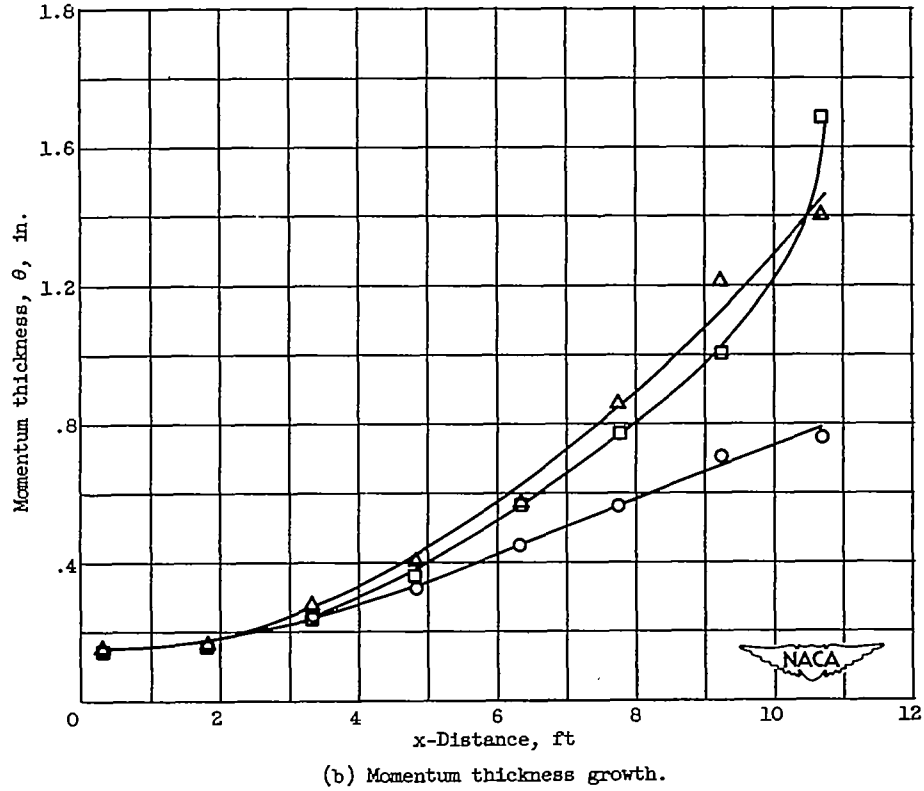

(b) Momentum thickness growth.

Figure 8. - Mean flow parameters along test wall.

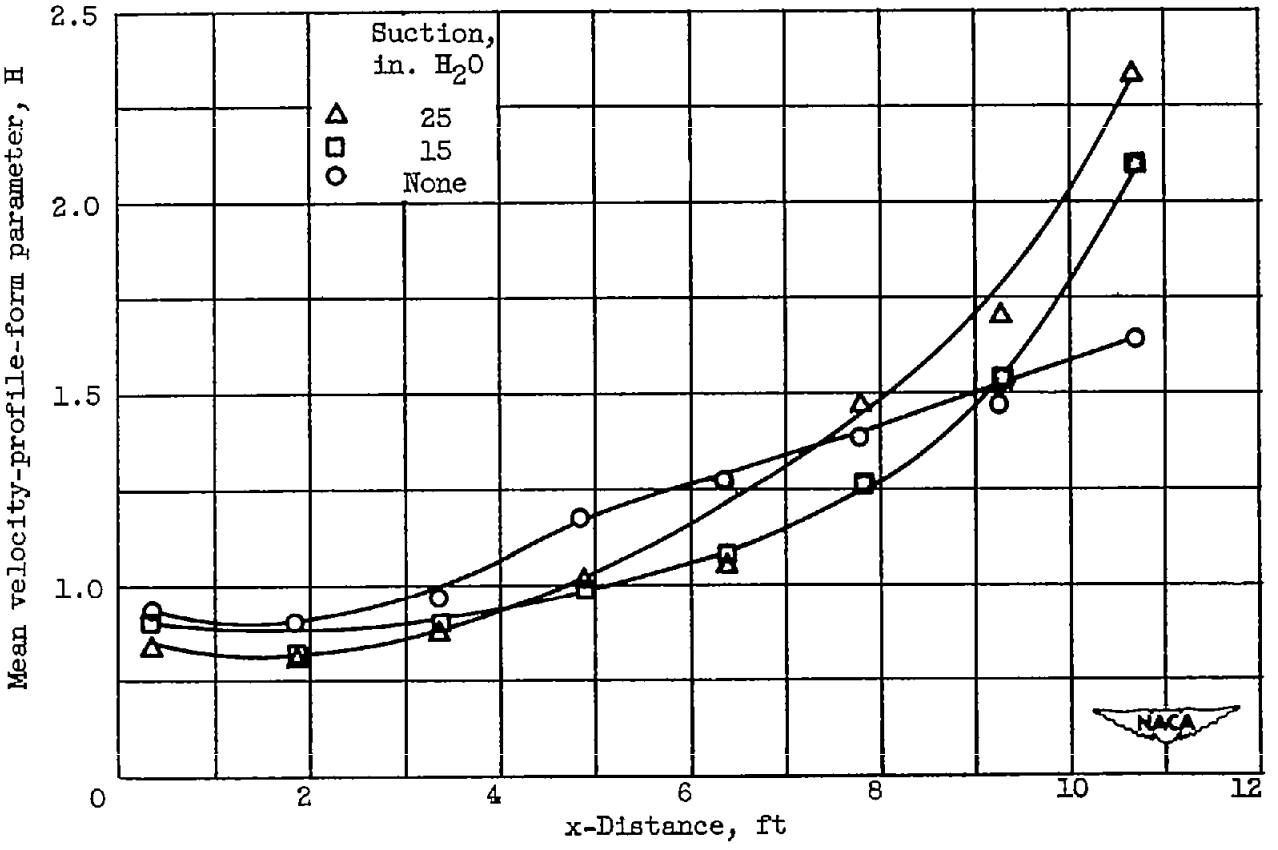

(c) Velocity-profile-form parameter growth.

Figure 8. - Concluded. Mean flow parameters along test wall.

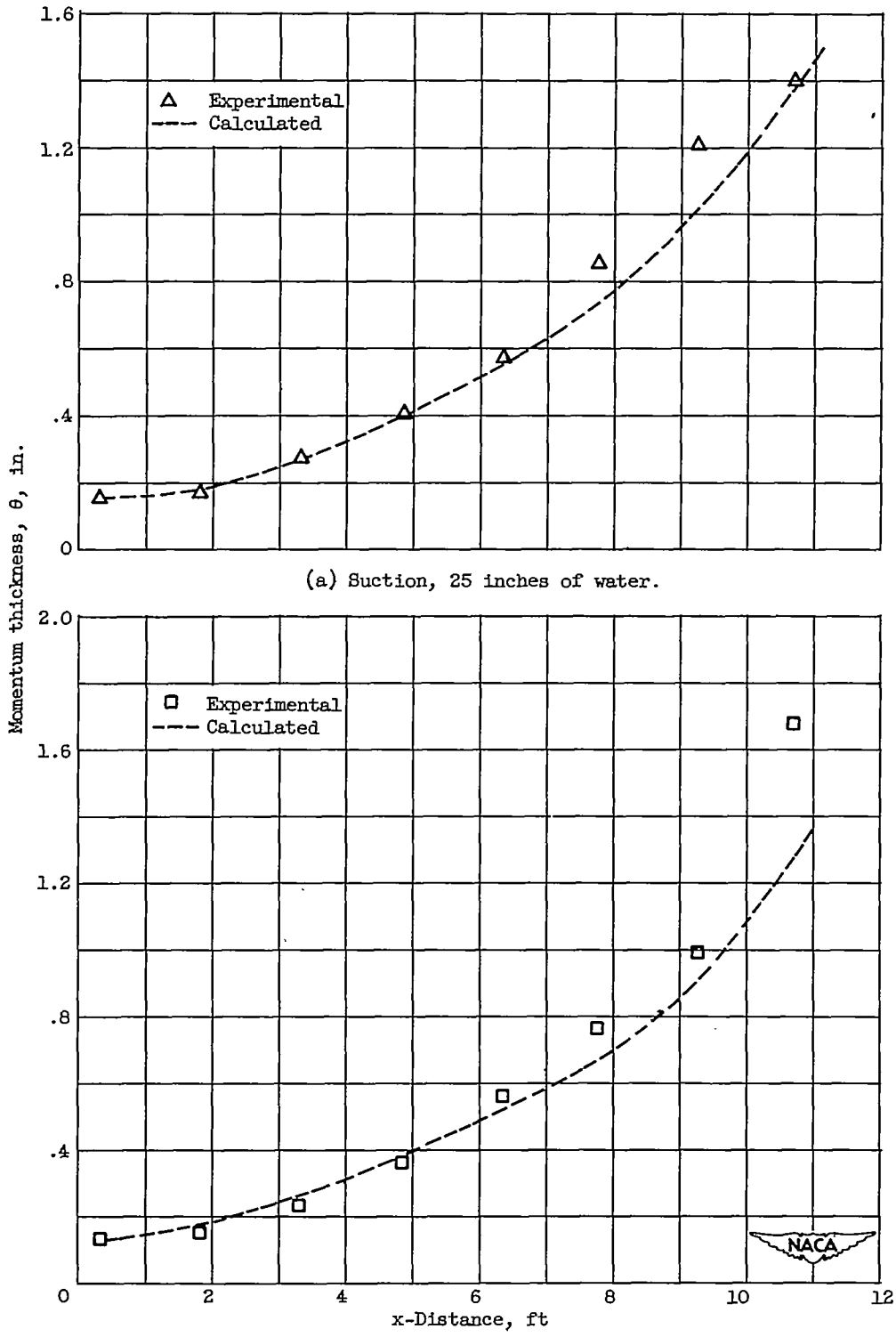

(a) Suction, 25 inches of water.

(b) Suction, 15 inches of water.

Figure 9. - Comparison of measured momentum thickness with value predicted from reference 6.

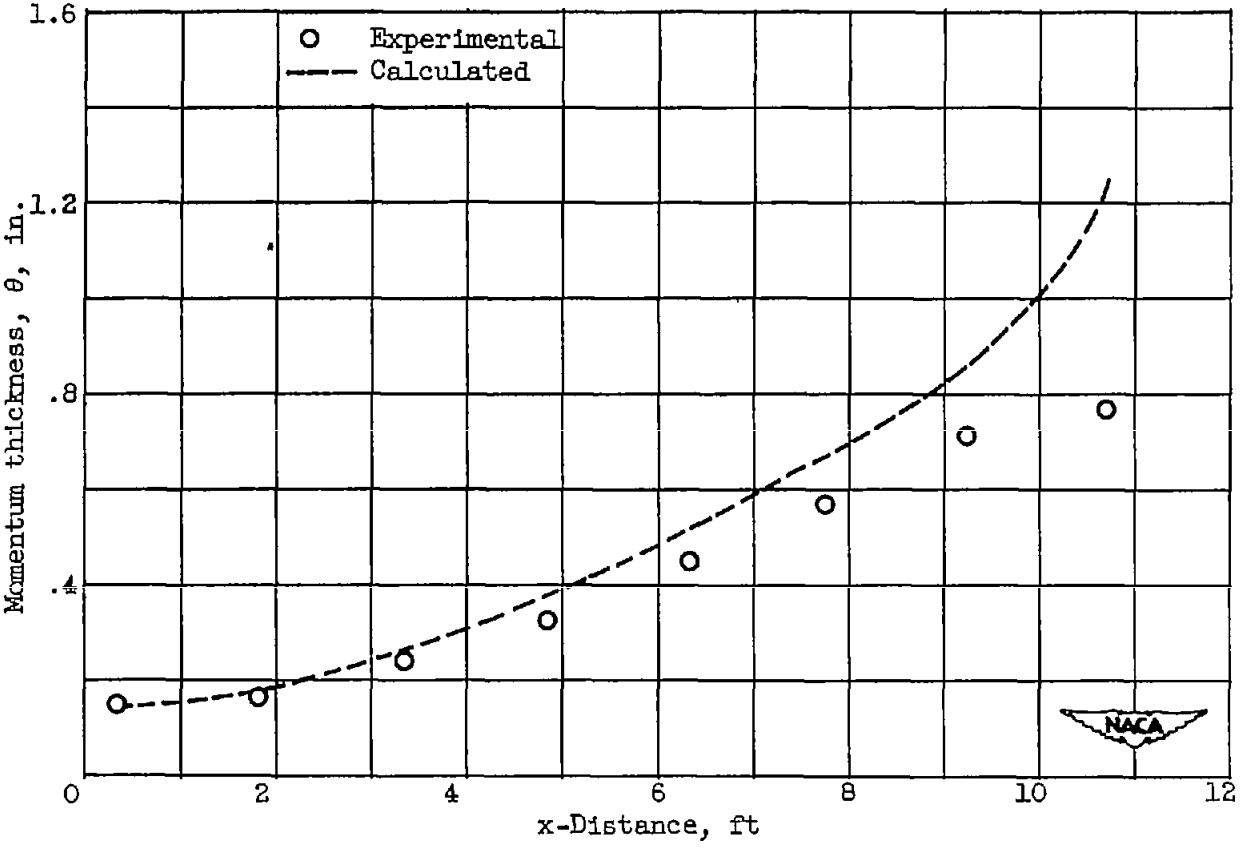

(c) No suction.

Figure 9. - Concluded. Comparison of measured momentum thickness with value predicted from reference 6.

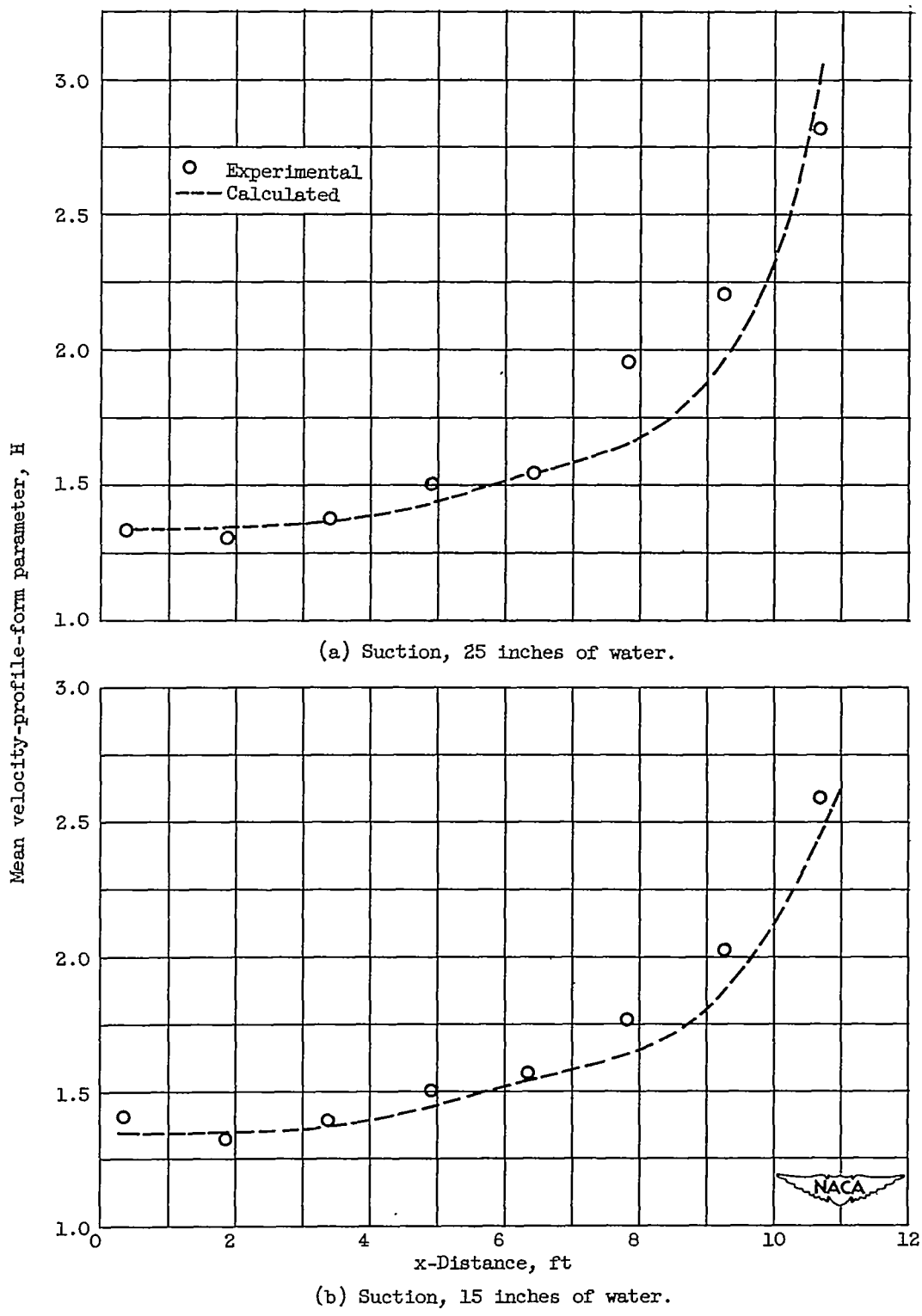

(a) Suction, 25 inches of water.

(b) Suction, 15 inches of water.

Figure 10. - Comparison of the measured mean velocity-profile-form parameter with predictions of reference 6.

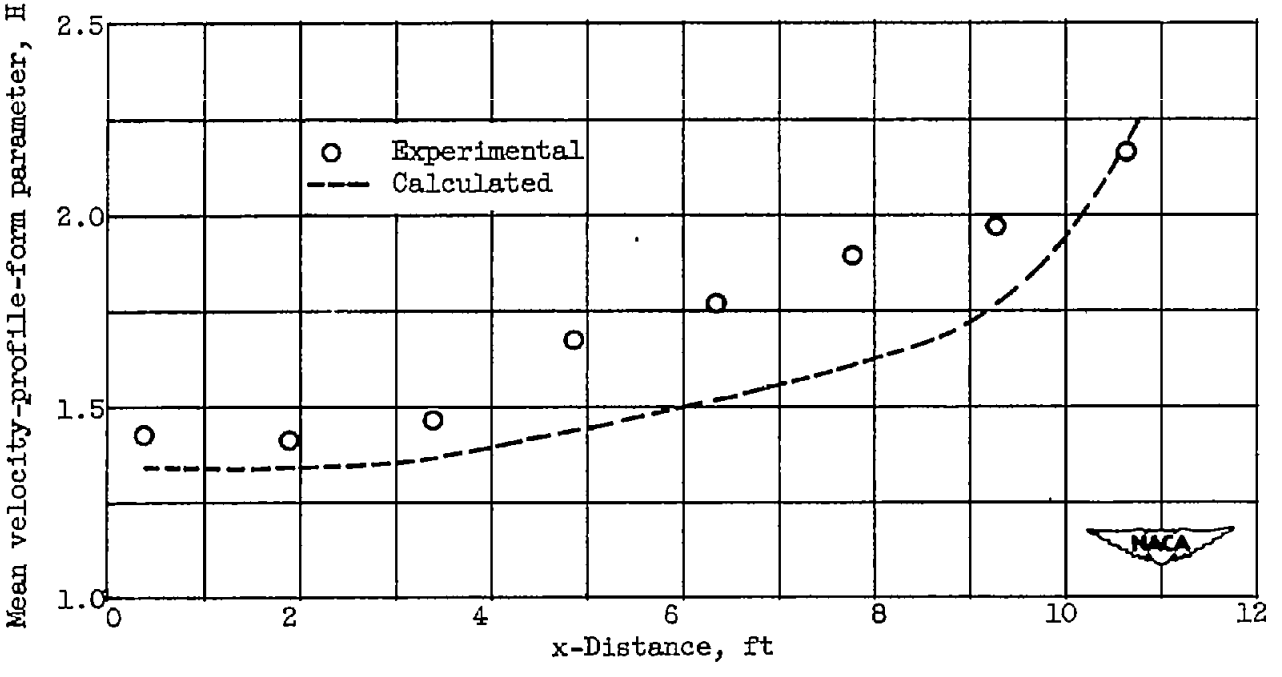

(c) No suction.

Figure 10. - Concluded. Comparison of the measured mean velocity-profile-form parameter with predictions of reference 6.

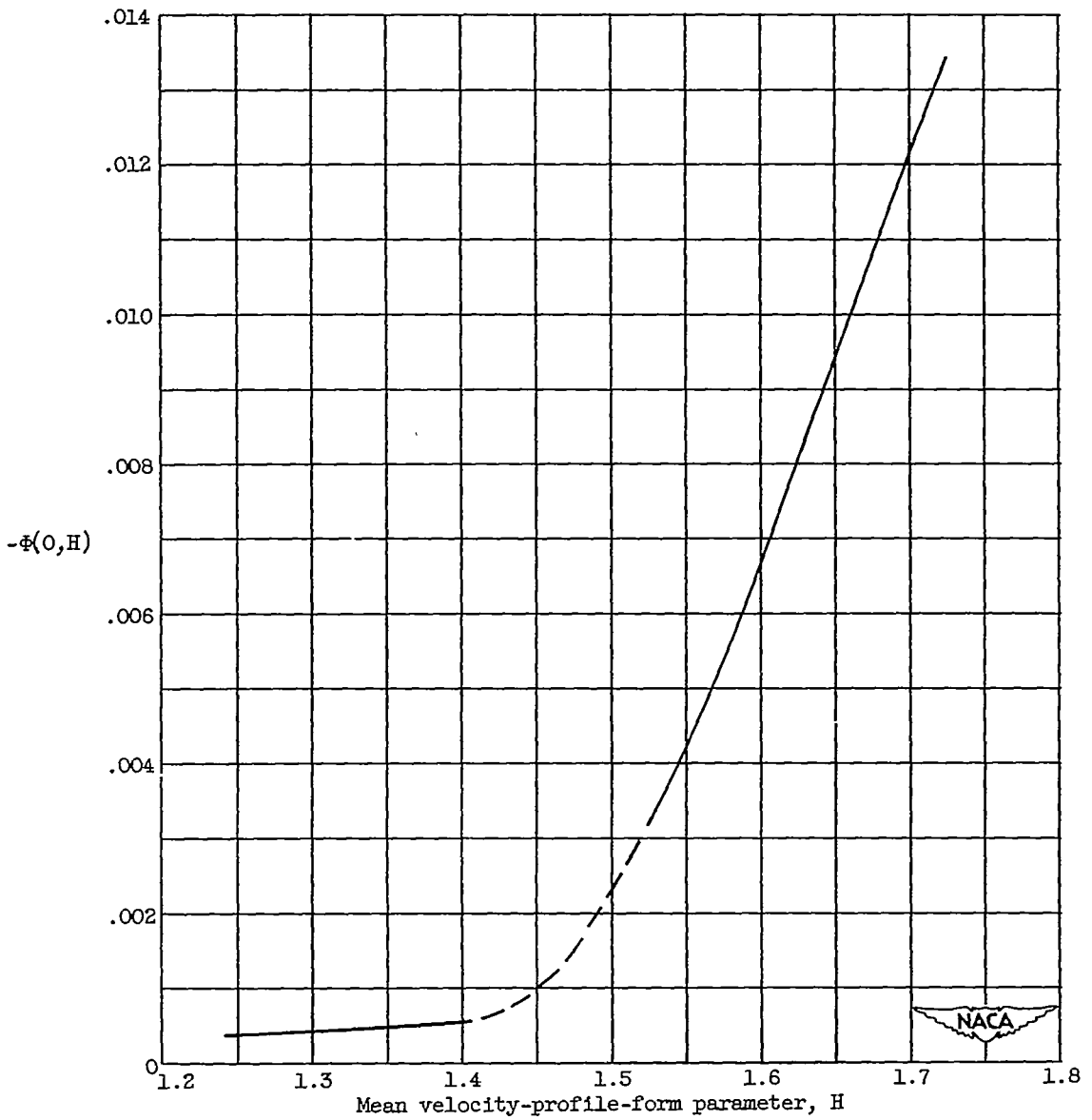

Figure 11. - Plot of function $\Phi(0,H)$ (reproduced from fig. 9 of ref. 6). For $H > 1.7$, use $-\Phi(0,H) = 0.054\,H - 0.0796$.

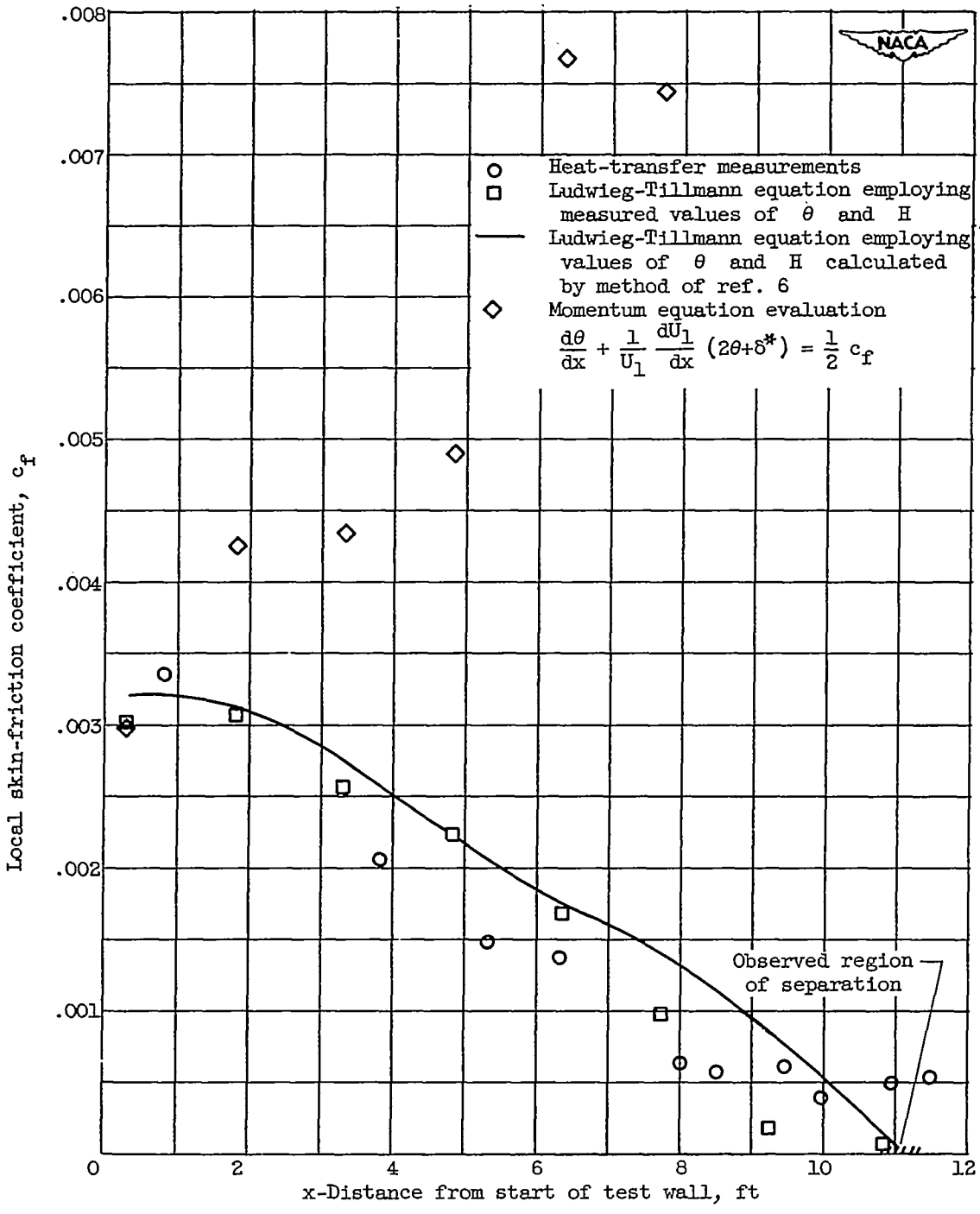

(a) Suction, 25 inches of water.

Figure 12. - Variation of local skin-friction coefficient along test wall.

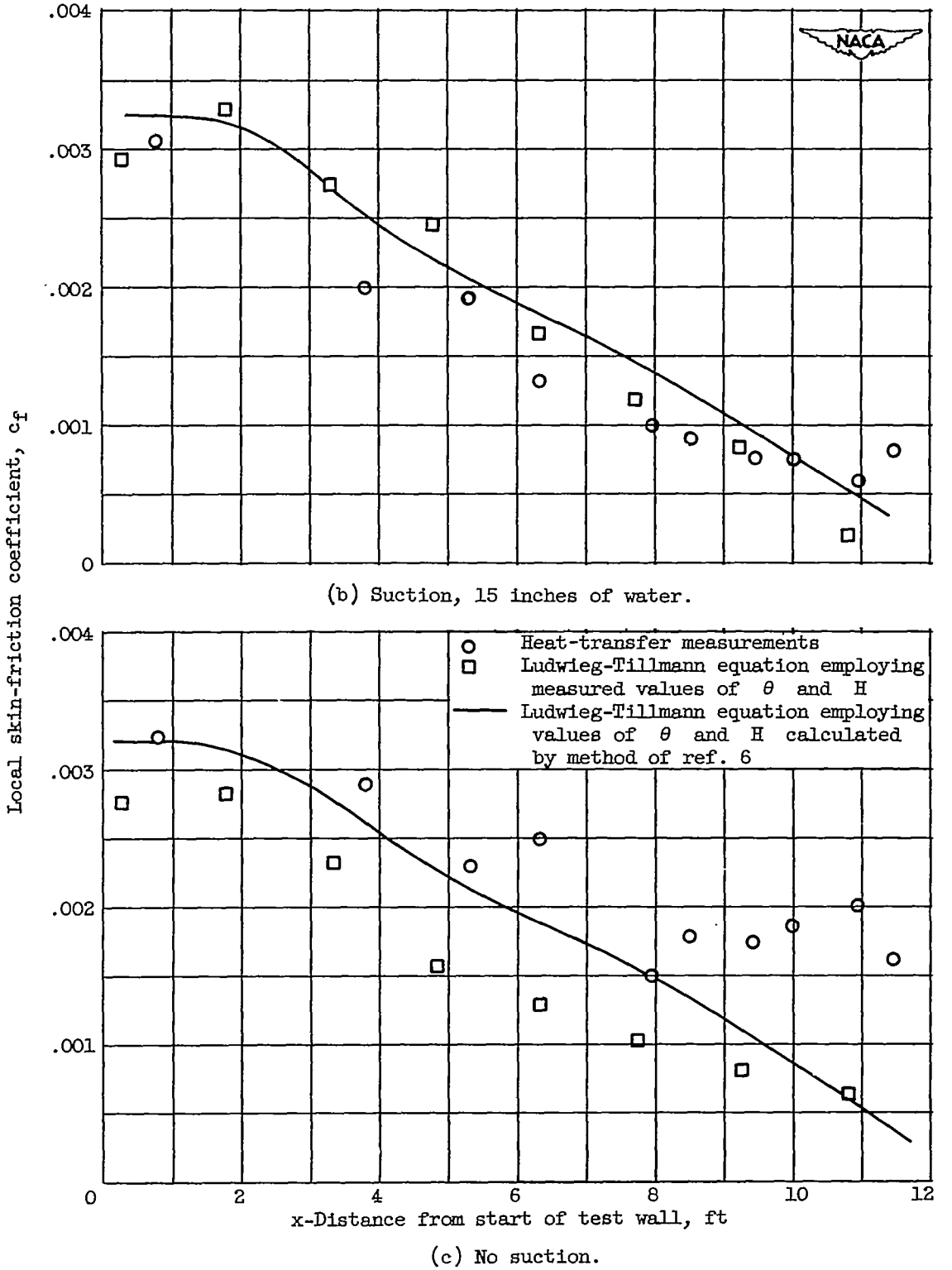

Figure 12. - Concluded. Variation of local skin-friction coefficient along test wall.

NACA-Langley - 10-15-53 - 1000